Microwave transitions from pairs of Rb $nd_{5/2}nd_{5/2}$ atoms

Jeonghun Lee* and T. F. Gallagher
Department of Physics, University of Virginia, Charlottesville, Virginia 22904-0714, USA
(Received 7 April 2016; published 20 June 2016)

We have observed resonant microwave transitions between pairs of atoms. Specifically, we have observed the processes $nd_{5/2}nd_{5/2} \rightarrow (n+1)d_j(n-2)f_{7/2}$ and $nd_{5/2}nd_{5/2} \rightarrow (n+2)p_{3/2}(n-1)d_{5/2}$ for $35 \leqslant n \leqslant 44$. These transitions are allowed due to the dipole-dipole-induced configuration interaction between the $nd_{5/2}nd_{5/2}$ state and the energetically nearby $(n+2)p_{3/2}(n-2)f_{7/2}$ state, which admixes some of the latter into the former. The resulting microwave transitions are analogous to two-photon transitions in which one of the photons has been replaced by the dipole-dipole interaction. We have developed a configuration interaction description of the transitions, which gives a good description of the interaction over the range $35 \leqslant n \leqslant 42$. Over this range of n the detuning varies from 0.095 to 1.482 GHz, the microwave frequencies vary from 26.970 to 45.916 GHz, and the requisite microwave powers vary by a factor of over 1000.

DOI: 10.1103/PhysRevA.93.062509

I. INTRODUCTION

There is substantial interest in molecules composed of one or more Rydberg atoms. The most well studied are the trilobite molecules in which a ground-state atom or molecule is bound to a Rydberg atom by its short-range interaction with the Rydberg electron [1–3]. Less well studied are molecules composed of more than one Rydberg atom. The first proposed were macrodimers based on the long-range van der Waals interactions of two Rydberg atoms in the same state [4,5]. Later proposals for even longer-range molecules were based on dipole-dipole interactions of atoms in different states [6,7]. While no experimental evidence for stable bound double Rydberg molecules has been presented, there is evidence for the existence of transient macrodimers. In laser excitation spectra, signatures of transient molecules formed by dipole-dipole, van der Waals, and dipole-quadrupole interactions have been observed [8–10]. Forster resonant energy transfer involving two, three, and even four atoms has been observed [11–14]. Finally, microwave transitions involving pairs of Rydberg atoms have been observed [15].

Here we report a systematic study of microwave transitions in which a pair of atoms absorbs a microwave photon, with the result that both atoms change state. Specifically, we have examined the process

$$nd_{5/2}nd_{5/2} \rightarrow (n+1)d_j(n-2)f_{7/2}. \tag{1}$$

Here n is the principal quantum number, and the molecular states are labeled by the atomic states of the two atoms. The process of Eq. (1) is observable due to the dipole-dipole configuration interaction (CI) between the $nd_{5/2}nd_{5/2}$ state and the energetically nearby $(n+2)p_{3/2}(n-2)f_{7/2}$ state:

$$nd_{5/2}nd_{5/2} \leftrightarrow (n+2)p_{3/2}(n-2)f_{7/2}. \tag{2}$$

For completeness, we have also verified that the molecular transition

$$nd_{5/2}nd_{5/2} \rightarrow (n+2)p_{3/2}(n-1)d_{5/2} \tag{3}$$

occurs due to the same CI. The CI-enabled microwave transition is roughly analogous to a two-photon transition, with the $(n+2)p_{3/2}(n-2)f_{7/2}$ state playing the role of the off-resonant intermediate state and the dipole-dipole interaction of Eq. (2) playing the role of one of the photons.

Systematic measurements of the microwave transition of Eq. (1) over the range $35 \leqslant n \leqslant 42$ show that the transition probability for the process of Eq. (1) can be described by a simple CI matrix element, in spite of the fact that over this range of n the microwave power required to drive the transition changes by more than three orders of magnitude. In the sections which follow we present a model for the transition of Eq. (1), describe our experimental procedure, and present our results.

II. CONFIGURATION-INTERACTION MODEL

The relevant energy levels for the microwave transition $nd_{5/2}nd_{5/2} \rightarrow (n+1)d_j(n-2)f_{7/2}$ are shown in Fig. 1. All other levels can be ignored. This transition is allowed because the $nd_{5/2}nd_{5/2}$ state is coupled to the nearby $(n+2)p_{3/2}(n-2)f_{7/2}$ state by the dipole-dipole interaction, shown by the double-headed dashed arrow in Fig. 1, and some of the $(n+2)p_{3/2}(n-2)f_{7/2}$ state is admixed into the $nd_{5/2}nd_{5/2}$ state. The dipole matrix element connecting the $nd_{5/2}$ state to the $(n-2)f_{5/2}$ state is a factor of 4 smaller than the one connecting it to the $(n-2)f_{7/2}$ state [16]. For this reason we see no evidence for transitions to final states containing an $(n-2)f_{5/2}$ state. At finite internuclear separation R, the $nd_{5/2}nd_{5/2}$ state can be written as

$$|nd_{5/2}nd_{5/2}\rangle_R = |nd_{5/2}nd_{5/2}\rangle + \epsilon|(n+2)p_{3/2}(n-2)f_{7/2}\rangle, \tag{4}$$

where the molecular states without the subscripts are the $R = \infty$ states and the admixture coefficient ϵ is given by

$$\epsilon = \frac{\langle nd_{5/2}nd_{5/2}|\mu\mu'|(n+2)p_{3/2}(n-2)f_{7/2}\rangle}{R^3\Delta} = \frac{\langle nd_{5/2}|\mu|(n+2)p_{3/2}\rangle\langle nd_{5/2}|\mu'|(n-2)f_{7/2}\rangle}{R^3\Delta}. \tag{5}$$

Here μ and μ' are the dipole moments of atoms 1 and 2. We ignore exchange effects. The admixture coefficient is the

*jl7rf@virginia.edu

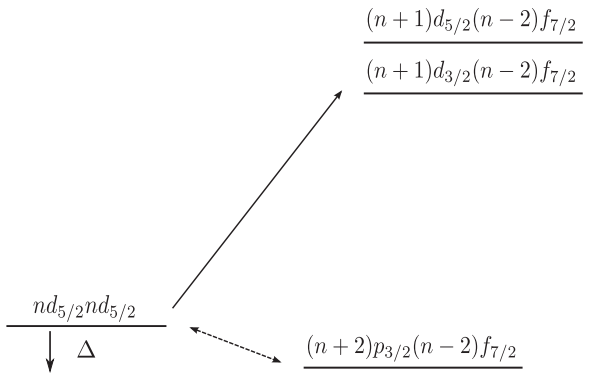

FIG. 1. Energy levels for the $nd_{5/2}nd_{5/2} \rightarrow (n+1)d_j(n-2)f_{7/2}$ microwave transition, shown by the solid arrow. This transition is allowed due to the configuration interaction between the $nd_{5/2}nd_{5/2}$ and $(n+2)p_{3/2}(n-2)f_{7/2}$ states, shown by the dashed double-headed arrow.

ratio of the dipole-dipole coupling to the energy detuning Δ between the $nd_{5/2}nd_{5/2}$ and $(n+2)p_{3/2}(n-2)f_{7/2}$ states at $R=\infty$, as shown in Fig. 1. Explicitly, the detuning is given by

$$\Delta = W_{nd_{5/2}nd_{5/2}} - W_{(n+2)p_{3/2}(n-2)f_{7/2}}. \tag{6}$$

The detunings between the $nd_{5/2}nd_{5/2}$ and $(n+2)p_{3/2}(n-2)f_{7/2}$ states are given in Table I. The energies of the atomic states have been calculated using the quantum defects given by Refs. [17,18]. The $nd_{5/2}nd_{5/2} - (n+1)d_j(n-2)f_{7/2}$ microwave transition matrix element is

$$\langle nd_{5/2}nd_{5/2}|_R \mu E|(n+1)d_j(n-2)f_{7/2}\rangle = \epsilon E \langle (n+2)p_{3/2}|\mu|(n+1)d_j\rangle \langle (n-2)f_{7/2}||(n-2)f_{7/2}\rangle, \tag{7}$$

where E is the microwave field amplitude. In this microwave transition, the $(n-2)f_{7/2}$ atom is a spectator. Since all the dipole matrix elements are approximately proportional to n^2, the microwave transition matrix element is given by

$$\langle nd_{5/2}nd_{5/2}|_R \mu E|(n+1)d_j(n-2)f_{7/2}\rangle = \frac{\beta n^6 E}{\Delta R^3}, \tag{8}$$

where β is a numerical constant of order 1.

TABLE I. Energy detunings Δ between the $nd_{5/2}nd_{5/2}$ and $(n+2)p_{3/2}(n-2)f_{7/2}$ states.

n	Δ (GHz)
34	1.8798
35	1.4820
36	1.1548
37	0.8849
38	0.6621
39	0.4778
40	0.3253
41	0.1991
42	0.09465
44	−0.06288

To compute the fractional population transfer (FPT) we follow an approach used by Pillet *et al.* [19]. Consider for a moment two $nd_{5/2}$ atoms separated by R. They are coupled to the $(n+1)d_j(n-2)f_{7/2}$ state by the coupling matrix element of Eq. (8), and a pair initially excited to the $nd_{5/2}nd_{5/2}$ state oscillates between it and the $(n+1)d_j(n-2)f_{7/2}$ state at the Rabi frequency Ω, given by

$$\Omega = \frac{\beta n^6 E}{|\Delta| R^3}. \tag{9}$$

If the microwave field is present for a time T, the $nd_{5/2}nd_{5/2}$ pair makes half a Rabi oscillation and is left in the $(n+1)d_j(n-2)f_{7/2}$ state if $\Omega T = \pi$, which occurs for $R = R_T$, where R_T is defined by

$$\Omega T = \frac{\beta n^6 E T}{|\Delta| R_T^3} = \pi. \tag{10}$$

If $R < R_T$ the pair oscillates more rapidly, and on average the probability of making the transition is $1/2$. On the other hand, if $R > R_T$, the probability of making the transition drops very rapidly due to the $1/R^3$ dependence of the coupling matrix element of Eq. (8). In sum, only pairs with $R < R_T$ undergo the transition. Assuming the fraction of pairs making the transition is small, the FPT from the $nd_{5/2}nd_{5/2}$ state to the $(n+1)d_j(n-2)f_{7/2}$ state is given by

$$\mathrm{FPT} = \frac{R_T^3}{R_{\mathrm{av}}^3}, \tag{11}$$

where R_{av} is the average spacing of the pairs, which is related to the density ρ by

$$\rho = \frac{3}{4\pi R_{\mathrm{av}}^3}. \tag{12}$$

We implicitly assume that $R_{\mathrm{av}} \gg R_{\mathrm{blockade}}$, where R_{blockade} is the radius of the blockade sphere [20]. This condition is easily met for our pulse amplified laser. Finally,

$$\mathrm{FPT} = \frac{\beta' n^6 E \rho}{|\Delta|}, \tag{13}$$

where $\beta' = 4\beta T/3$. The fractional population transfer is bilinear in the density of the Rydberg atoms and the microwave field amplitude. As n is changed from 35 to 42, n^6/Δ changes by a factor of 50. Therefore, at a constant density ρ the microwave power needed to observe the same fractional population transfer should change by a factor of 2500.

While it is straightforward to make relative microwave field or power measurements at a fixed frequency, comparing the microwave fields over the broad frequency range we have used presents more of a problem since we do not know how efficiently the microwave power is transmitted to the interaction region from the horn. The ac Stark shift of the observed resonances, analogous to that observed in two-photon spectroscopy, provides a way to calibrate absolutely the microwave field. The $nd_{5/2}nd_{5/2} - (n+1)d_{5/2}(n-2)f_{7/2}$ transition is nearly resonant with the atomic $(n+2)p_{3/2} - (n+1)d_j$ transition, and the ac Stark shift of these two atomic levels shifts the $(n+1)d_j(n-2)f_{7/2}$ and $(n+2)p_{3/2}(n-2)f_{7/2}$ states in opposite directions, as shown in Fig. 2, which is drawn for $\Delta > 0$.

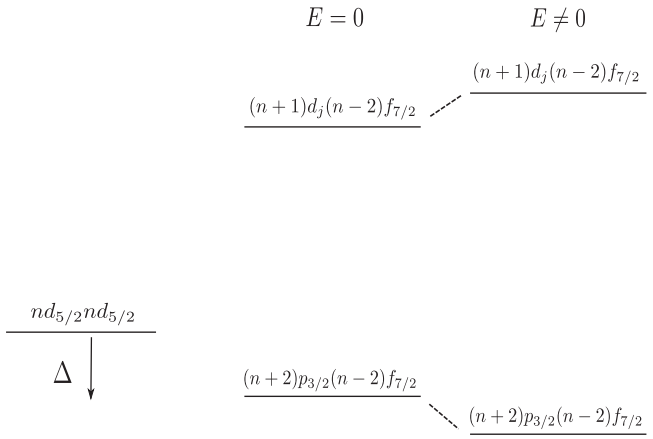

FIG. 2. The ac Stark shift of the $(n+1)d_j(n-2)f$ and $(n+2)p_{3/2}(n-2)f_{7/2}$ states.

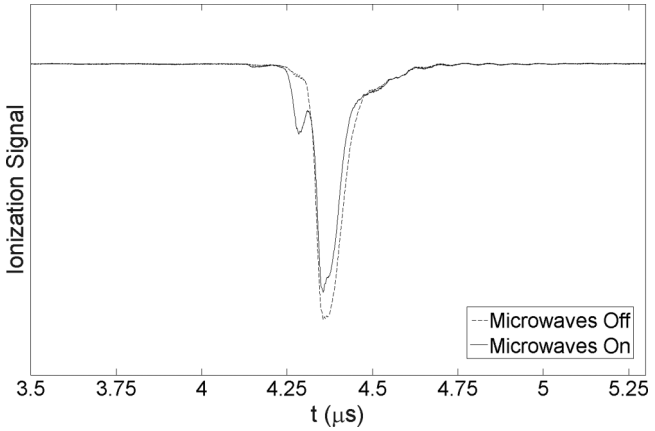

FIG. 3. Field-ionization signal for the $39d_{5/2}39d_{5/2} \rightarrow 40d_{5/2}37f_{7/2}$ transition with microwaves off (dashed line) and microwaves on (solid line). The microwaves are tuned to 33.613 GHz, the resonance frequency for the $39d_{5/2}39d_{5/2} \rightarrow 40d_{5/2}37f_{7/2}$ transition.

For a linearly polarized microwave field the azimuthal angular momentum number m_j is fixed, and there are two ac Stark shifts, for $|m_j| = 1/2$ and $3/2$. The Stark shifts of the $(n+1)d_j(n-2)f_{7/2}$ state are easily calculated using a Floquet approach and are given by [21]

$$\Delta W_{(n+1)d_j(n-2)f_{7/2}} = \frac{[\langle (n+1)d_{5/2}m_j|\mu_z|(n+2)p_{3/2}m_j\rangle E]^2}{4\Delta}. \quad (14)$$

For $|m_j| = 1/2$ and $3/2$ the Stark shifts are given by

$$\Delta W_{(n+1)d_j(n-2)f_{7/2}} = \frac{\gamma n^4 E^2}{\Delta}, \quad (15)$$

with $\gamma = 0.0801$ and 0.0534 for $|m_j| = 1/2$ and $3/2$, respectively, when $n = 39$. The constant γ includes all the angular factors and the scaling of the radial matrix elements, and γ ranges from 0.07997 to 0.0802 for $|m_j| = 1/2$ and 0.05331 to 0.05347 for $|m_j| = 3/2$ as n is increased from 35 to 42. The radial matrix elements for $\langle (n+1)d_{5/2}|\mu_z|(n+2)p_{3/2}\rangle$ are given in Ref. [22].

III. EXPERIMENTAL APPROACH

In the experiment ^{85}Rb atoms are trapped in a magneto-optical trap (MOT) which is vapor loaded. The MOT provides a steady population of Rb atoms in the $5p_{3/2}$ state. Atoms are excited to the $nd_{5/2}$ state by a 10-μJ 480-nm laser pulse which is generated by pulse amplifying, at a 20-Hz repetition rate, the output of tapered amplifier seeded by a 960-nm diode laser and then frequency doubling it. The optical pulse is 10 ns long and has a bandwidth of 150 MHz. Approximately 4 ms before the pulsed laser excitation, the trap magnetic fields are switched off to reduce the residual field in the MOT to less than 50 mG during the experiment. Subsequent to laser excitation, the atoms are exposed to a 1-μs-long microwave pulse to drive the $nd_{5/2}nd_{5/2} \rightarrow (n+1)d_j(n-2)f_{7/2}$ or $nd_{5/2}nd_{5/2} \rightarrow (n+2)p_{3/2}(n-1)d_{5/2}$ transition. Fifty nanoseconds after the end of the microwave pulse, a 700-ns-rise-time voltage pulse is applied to the rods to field ionize the Rydberg atoms and drive the resulting ions to a microchannel plate (MCP) detector. The signal from the MCP is recorded with either a gated integrator or an oscilloscope and is stored in a computer for later analysis.

The cloud of cold Rb atoms is held at the center of four vertical rods which pass through the corners of a horizontal square 18 mm on a side. The rods allow the application of the field-ionization pulse. The density of Rydberg atoms in the MOT is determined in the following way. The 780-nm fluorescence from the MOT is measured to find the total number of the trapped $5p$ atoms. Then, the number of Rydberg atoms excited on each laser shot can be determined by combining the measured reduction of the $5p$ population when the pulsed Rydberg excitation is added and the 1-s filling time of the trap. The density of the Rydberg atoms is determined by measuring the waist of the 480-nm beam and the diameter of the MOT. We assume the Rydberg atom density to have the following form: $\rho(x,y,z) = \rho_0 e^{-(x^2+y^2+z^2)/r_M^2} e^{-(x^2+y^2)/r_L^2}$, where $r_M = 0.5$ mm and $r_L = 0.18$ mm are the radii of the MOT and the 480-nm laser beam, respectively; ρ_0 is the density at the center of the trap; and x, y, and z are the Cartesian displacements from the center of the trap. The 480-nm beam propagates in the z direction. In these experiments, the maximum value of ρ_0 is 4×10^8 cm^{-3}, and the density measurement uncertainty is a factor of 3.

The microwaves are generated in an Agilent 83622B synthesizer, which has a maximum frequency of 20 GHz, and a General Microwave DM862B switch is used to form the microwaves into 1-μs-long pulses. A Hewlett Packard (HP) 83554A passive doubler is used for the 26.5- to 40-GHz range, covering $37 \leqslant n \leqslant 44$, and a Narda DBS4060X410 active quadrupler is used for the 40- to 60-GHz range, covering $35 \leqslant n \leqslant 37$. The relative microwave power is controlled in the final waveguide with a HP R832A or U832A precision attenuator. The microwaves have horizontal polarization and propagate from a horn outside the vacuum system through a window to the MOT volume. The vertical rods used to apply the field-ionization pulse scatter the microwaves to some extent, and this may result in the polarization's not being perfectly linear. As mentioned earlier, there is an ac Stark shift due to near resonance of the microwaves to the $(n+2)p_{3/2} \rightarrow$

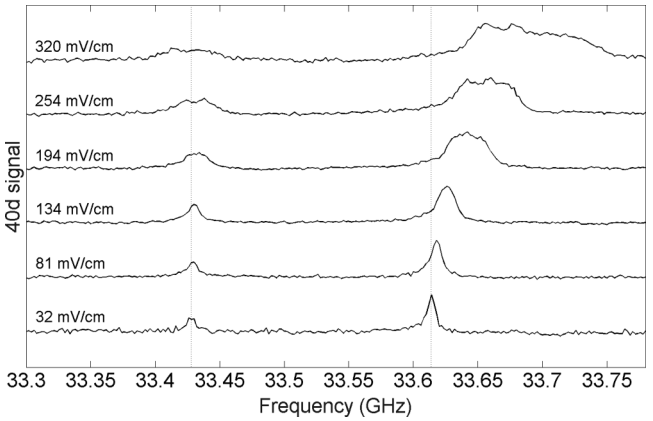

FIG. 4. Observed $39d_{5/2}39d_{5/2} \rightarrow 40d_j37f_{7/2}$ resonances for a range of microwave field amplitudes. The dotted lines represent the calculated resonance frequencies for the transitions at zero microwave power and $R = \infty$.

$(n+1)d_j$ transition. It is straightforward to extrapolate the location of the resonance peaks to zero microwave power, and the power shift is used to calibrate absolutely the microwave fields over the range of frequencies employed.

To field ionize atoms in states above $n = 41$ we apply a positive voltage pulse to the rods farther from the MCP while the two rods nearer the MCP are grounded. To ionize atoms in states of $37 \leqslant n \leqslant 41$ we also apply a negative voltage pulse with the same 700-ns rise time to the rods nearer to the MCP. This two-pulse scheme is implemented because the output of one circuit for generating the pulse with a rapid initial rise is limited to 500 V, which is not enough to ionize the Rydberg states of $n \leqslant 41$. The field-ionization pulse has a rapid initial rise and is similar to the fast pulse used for the experiment by Han and Gallagher [23]. Using this type of pulse with rapid initial rise allows us to suppress adiabatic transitions through molecular avoided crossings on the rising edge of the field pulse. Such transitions, which occur with slowly rising field pulses [23–26], lead to field-ionization signals almost identical to the resonant signals we wish to detect. Since they originate from pairs of closely spaced atoms, they artificially suppress

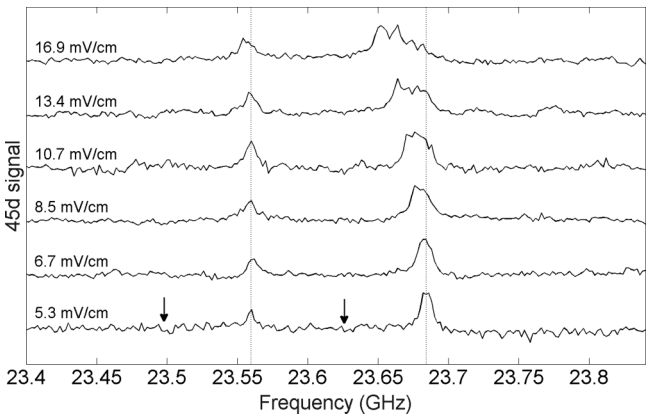

FIG. 5. Observed $44d_{5/2}44d_{5/2} \rightarrow 45d_j42f_{7/2}$ resonances for a range of microwave field amplitudes. The dotted lines represent the calculated resonance frequencies for the transitions at zero microwave power and $R = \infty$.

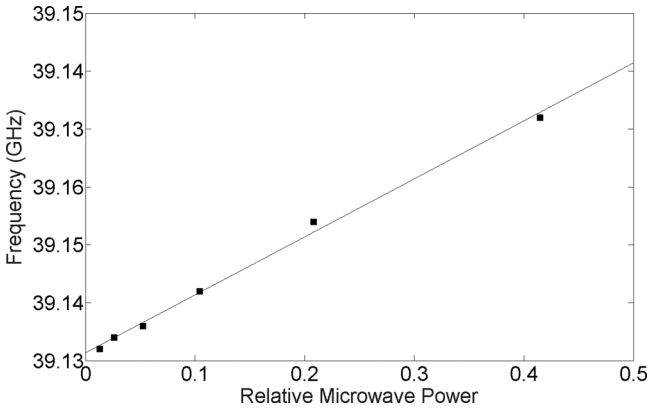

FIG. 6. Resonance frequency vs microwave power for the $37d_{5/2}37d_{5/2} \rightarrow 38d_{5/2}35f_{7/2}$ transition.

the resonant signals due to the processes of Eqs. (1) and (3). For $35 \leqslant n \leqslant 37$ we have used a field-ionization pulse which has a higher amplitude but a slow initial rise [23].

IV. OBSERVATIONS AND DISCUSSION

Our signals are time-resolved, state-selective field-ionization signals. As an example, ionization signals from atoms excited to $39d_{5/2}$ with no microwaves (dashed line) and with microwaves tuned to the $39d_{5/2}39d_{5/2} \rightarrow 40d_{5/2}37f_{7/2}$ resonance (solid line) are shown in Fig. 3. Time $t = 0$ is when the field-ionization circuit is triggered. The large peak at $t = 4.36\ \mu$s is from atoms in the $39d_{5/2}$ state. With microwaves on, a peak earlier in time at $t = 4.29\ \mu$s, corresponding to atoms in the $40d_{5/2}$ state, appears, and a decrease in the $39d_{5/2}$ signal is observed. Careful examination of Fig. 3 reveals a small signal at $t = 4.29\mu s$ with no microwaves due to the nonadiabatic transitions during the field pulse.

By setting the gate of the integrator on the $40d_j$ signal at $t = 4.29\ \mu$s and sweeping the microwave frequency over many shots of the laser we obtain the $39d_{5/2}39d_{5/2} \rightarrow 40d_j37f_{7/2}$ traces of Fig. 4, which show the resonances for a range of microwave field amplitudes. There is no signal at the

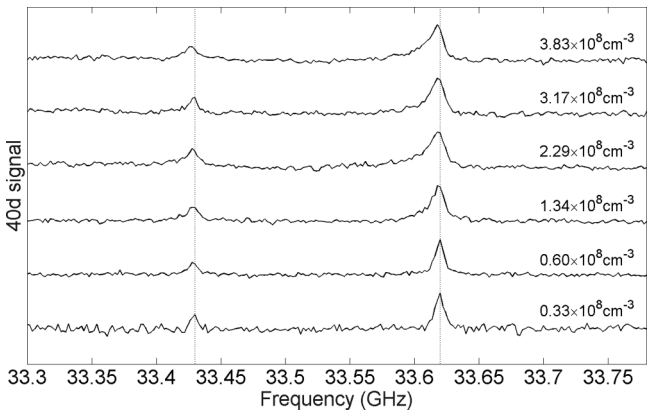

FIG. 7. Observed $39d_{5/2}39d_{5/2} \rightarrow 40d_j37f_{7/2}$ resonances for a range of peak Rydberg atom densities. The dotted lines represent the calculated resonance frequencies for the transition at zero microwave power and $R = \infty$.

TABLE II. Resonance frequencies for the $nd_{5/2}nd_{5/2} \rightarrow (n+1)d_{5/2}(n-2)f_{7/2}$ transitions.

n	Calculated (MHz)	Observed (MHz)	Difference (MHz)
34	49897.9	49898.4	0.5
35	45916.0	45915.0	1.0
36	42344.0	42341.0	3.0
37	39131.0	39130.7	0.3
38	36233.3	36232.8	0.5
39	33613.3	33613.6	−0.3
40	31238.7	31238.3	0.4
41	29081.9	29080.0	1.9
42	27117.9	27116.0	1.9
44	23688.6	23689.6	−1.0

frequencies of the $41p_{3/2} \rightarrow 40d_{3/2}$ and $41p_{3/2} \rightarrow 40d_{5/2}$ atomic transitions (Those atomic transitions are not within the scan range for Fig. 4). As the microwave field amplitude is raised, the transitions exhibit ac Stark shifts to higher frequency as well as splitting and broadening. The origin of the ac Stark shift is the near resonance with the atomic $41p_{3/2} - 40d_j$ transition. We attribute the splitting to the difference in the ac Stark shifts of the $40d_{5/2}$ state of $|m_j| = 1/2$ and $|m_j| = 3/2$, as discussed earlier. The broadening is due, at least in part, to inhomogeneities in the microwave field. The relative microwave fields of the traces shown in Fig. 4 are easily determined from the setting of the attenuator, and the absolute fields are determined by comparing the observed shifts to those calculated assuming the shifts to originate from the $41p_{3/2} - 40d_j$ transitions, as described in an earlier section.

Figure 5 shows the $45d$ signal vs microwave frequency for the $44d_{5/2}44d_{5/2} \rightarrow 45d_j42f$ transitions for a range of microwave field amplitudes. Again, there is no signal at the frequencies of the $46p_{3/2} \rightarrow 45d_{3/2}$ and $46p_{3/2} \rightarrow 45d_{5/2}$ atomic transitions, indicated by the arrows. For $n = 44$, $\Delta < 0$ and an ac Stark shift of the resonances in the opposite direction is observed. As in Fig. 4, the relative microwave fields are determined from the attenuator, and they are put on an absolute basis using the ac Stark shift.

To obtain the zero-microwave-power resonance frequency for a transition, the frequency of the resonance peak at different microwave field amplitudes is extrapolated back to zero power. Figure 6 shows an example of the extrapolation for the $37d_{5/2}37d_{5/2} \rightarrow 38d_{5/2}35f_{7/2}$ transition. Tables II and III give the zero-microwave-power frequencies for our measurements. All frequencies agree well with the calculated $R \rightarrow \infty$ values, which are calculated using the quantum defects of Refs. [17,18].

TABLE III. Resonance frequencies for the $nd_{5/2}nd_{5/2} \rightarrow (n+1)d_{3/2}(n-2)f_{7/2}$ transitions.

n	Calculated (MHz)	Observed (MHz)	Difference (MHz)
34	49618.3	49617.4	0.9
35	45659.8	45659.6	0.2
36	42108.8	42106.2	2.6
37	38914.4	38911.9	2.5
38	36033.5	36030.8	2.7
39	33428.6	33427.7	0.9
40	31067.6	31066.2	1.4
41	28922.9	28920.6	2.3
42	26970.2	26968.2	2.0
44	23560.3	23563.0	−2.7

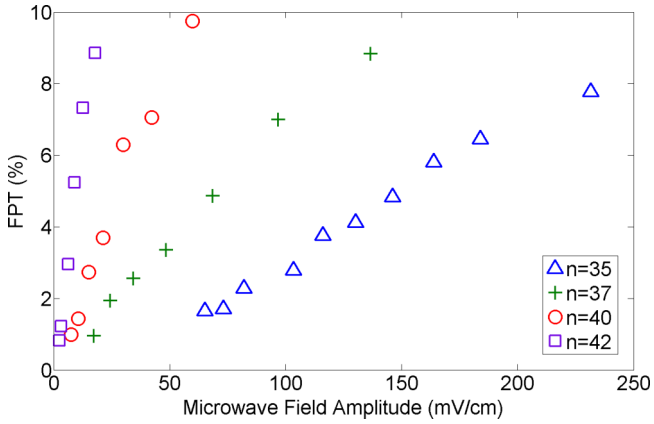

FIG. 8. FPT vs microwave field amplitude for $n = 35$ (△), $n = 37$ (+), $n = 40$ (○), and $n = 42$ (□) at similar densities of $\rho_0 = 1.7 \times 10^8$ cm^{-3}.

While there is an evident microwave power shift, there is minimal shift with Rydberg atom density. As an example, Fig. 7 shows scans of the $40d_j$ signal vs microwave frequency for the $39d_{5/2}39d_{5/2} \rightarrow 40d_j37f_{7/2}$ transitions for a range of Rydberg atom densities.

To test the CI model we have measured the FPT from the $nd_{5/2}nd_{5/2}$ to the $(n+1)d_j(n-2)f_{7/2}$ states. The model is valid for small FPT. At very high densities other processes begin to occur. For example, transfer to not only the $(n+1)d_j$ state but also the $(n+2)d_j$ state is observed. Accordingly, we have kept the density below $\rho_0 = 5 \times 10^8$ cm^{-3}, where the observations are consistent with our CI model. To measure the FPT for $37 \leqslant n \leqslant 42$, the ratio of the increase in the $(n+1)d_j$ signal when microwaves are tuned to resonance to the area of the $nd_{5/2}$ signal without the microwaves is used. For $n = 44$ even with the fast field-ionization pulse there is appreciable population transfer to higher-lying states in the field pulse,

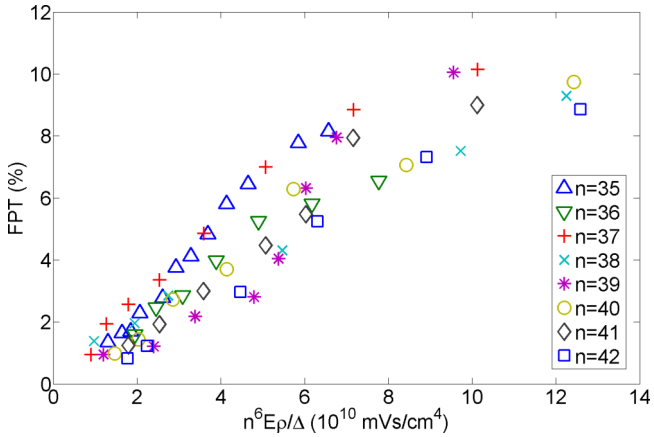

FIG. 9. FPT vs $\frac{n^6\rho E}{\Delta}$ for $35 \leqslant n \leqslant 42$.

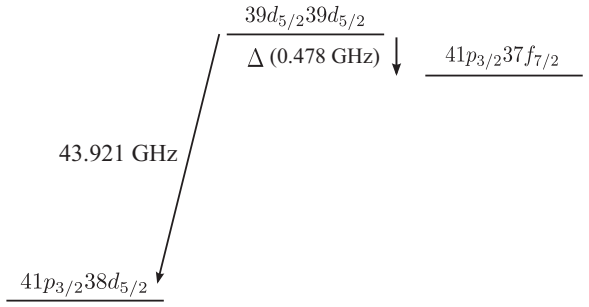

FIG. 10. Energy-level diagram for the $39d_{5/2}39d_{5/2} \rightarrow 41p_{3/2}38d_{5/2}$ transition.

so we do not include $n = 44$ in the FPT measurements. For $35 \leqslant n \leqslant 37$ we have used the higher-amplitude slow field-ionization pulse and measured the depletion of the $nd_{5/2}$ signal with the microwaves at the resonance frequency. For $n = 37$, the state for which the FPT was measured both ways, the fractional depletion of the $37d_{5/2}$ signal is slightly over twice as large as the increase in the $38d_j$ signal (A factor of 2 is expected since population must go down in energy to the $35f_{7/2}$ state). Using the same factor used to normalize the $n = 37$ depletion data, we normalize the $n = 35$ and 36 depletion data for inclusion in Figs. 8 and 9. For each state, the absolute microwave field amplitude is obtained by using the ac Stark shift, as described previously.

Figure 8 shows the FPT vs microwave field amplitude for $n = 35$, 37, 40, and 42 at similar densities of $\rho_0 = 1.7 \times 10^8$ cm^{-3}. Between $n = 35$ and 42, the microwave field amplitude required to produce the same FPT drops by more than a factor of 30. As suggested by Eq. (13), plotting the FPT vs $\frac{n^6 \rho E}{|\Delta|}$ should result in the data points' falling on the same straight line. As shown by Fig. 9, the points are close to falling on the same line, but at higher n the points are systematically low. This deviation from the expectation based on Eq. (13) may be due to a slightly larger adiabatic population transfer to higher n during the field pulse, which is more likely at higher n and suppresses the resonant signal. It is primarily the decrease in Δ which leads to the larger adiabatic transfer as n is raised. In any event, Fig. 9 demonstrates that the CI description of the process is quite good.

Since the CI couples the $nd_{5/2}nd_{5/2}$ state to the $(n+2)p_{3/2}(n-2)f_{7/2}$ state, it should be possible to drive transitions in which the $(n-2)f_{7/2}$ atom undergoes the transition while the $(n+2)p_{3/2}$ atom is a spectator, as shown by the energy-level diagram in Fig. 10. To verify that such transitions are possible we have driven the $39d_{5/2}39d_{5/2} \rightarrow 41p_{3/2}38d_{5/2}$ transition of Fig. 10. As shown in Fig. 10, the transition is to a

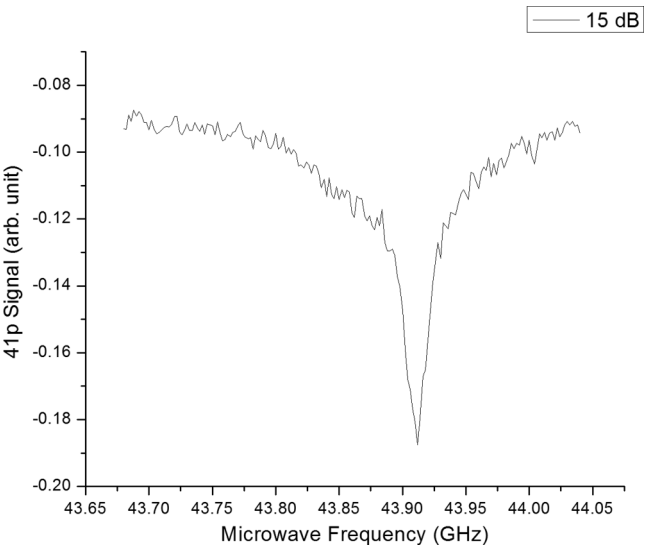

FIG. 11. Observed $39d_{5/2}39d_{5/2}$ to $41p_{3/2}38d_{5/2}$ transition.

molecular state lower in energy, but the atomic $41p_{3/2}$ state lies above the initial $39d_{5/2}$ state, so at resonance the $41p_{3/2}$ signal appears earlier in time than the $39d_{5/2}$ signal, approximately as shown in Fig. 3. The observed resonance is shown in Fig. 11. The location of the peak, at 43.922 GHz (extrapolated to zero microwave power), is in good agreement with the calculated $R = \infty$ interval of 43.9213 GHz. However, the origin of the pedestal seen in Fig. 11 is not yet understood.

V. CONCLUSION

We have observed resonant microwave transitions between pairs of atoms in which a single microwave photon is absorbed yet both of the constituent atoms in the molecule change state. Specifically, we have observed the processes $nd_{5/2}nd_{5/2} \rightarrow (n+1)d_j(n-2)f_{7/2}$ and $nd_{5/2}nd_{5/2} \rightarrow (n+2)p_{3/2}(n-1)d_{5/2}$. These transitions are allowed due to the dipole-dipole-induced configuration interaction between the $nd_{5/2}nd_{5/2}$ state and the energetically nearby $(n+2)p_{3/2}(n-2)f_{7/2}$ state, which admixes some of the latter into the former. The strengths of the transitions are in good agreement with a simple CI description of the process.

ACKNOWLEDGMENTS

It is a pleasure to acknowledge helpful discussions with H. Park, R. R. Jones, and P. Pillet and the support of the Air Force Office of Scientific Research under Grant No. FA9550-14-1-0288.

[1] C. H. Greene, A. S. Dickinson, and H. R. Sadeghpour, Phys. Rev. Lett. **85**, 2458 (2000).

[2] V. Bendkowsky, B. Butscher, J. Nipper, J. P. Shaffer, R. Löw, and T. Pfau, Nature (London) **458**, 1005 (2009).

[3] J. Tallant, S. T. Rittenhouse, D. Booth, H. R. Sadeghpour, and J. P. Shaffer, Phys. Rev. Lett. **109**, 173202 (2012).

[4] C. Boisseau, I. Simbotin, and R. Côté, Phys. Rev. Lett. **88**, 133004 (2002).

[5] N. Samboy, J. Stanojevic, and R. Côté, Phys. Rev. A **83**, 050501 (2011).

[6] M. Kiffner, H. Park, W. Li, and T. F. Gallagher, Phys. Rev. A **86**, 031401 (2012).

[7] M. Kiffner, W. Li, and D. Jaksch, Phys. Rev. Lett. **111**, 233003 (2013).
[8] S. M. Farooqi, D. Tong, S. Krishnan, J. Stanojevic, Y. P. Zhang, J. R. Ensher, A. S. Estrin, C. Boisseau, R. Côté, E. E. Eyler, and P. L. Gould, Phys. Rev. Lett. **91**, 183002 (2003).
[9] K. R. Overstreet, A. Schwettmann, J. Tallant, D. Booth, and J. P. Shaffer, Nat. Phys. **5**, 581 (2009).
[10] J. Deiglmayr, H. Saßmannshausen, P. Pillet, and F. Merkt, Phys. Rev. Lett. **113**, 193001 (2014).
[11] I. Mourachko, D. Comparat, F. de Tomasi, A. Fioretti, P. Nosbaum, V. M. Akulin, and P. Pillet, Phys. Rev. Lett. **80**, 253 (1998).
[12] W. R. Anderson, J. R. Veale, and T. F. Gallagher, Phys. Rev. Lett. **80**, 249 (1998).
[13] J. H. Gurian, P. Cheinet, P. Huillery, A. Fioretti, J. Zhao, P. L. Gould, D. Comparat, and P. Pillet, Phys. Rev. Lett. **108**, 023005 (2012).
[14] R. Faoro, B. Pelle, A. Zuliani, P. Cheinet, E. Arimondo, and P. Pillet, Nat. Commun. **6**, 8173 (2015).
[15] Y. Yu, H. Park, and T. F. Gallagher, Phys. Rev. Lett. **111**, 173001 (2013).
[16] A. Edmonds, *Angular Momentum in Quantum Mechanics* (Princeton University Press, Princeton, NJ, 1960).
[17] W. Li, I. Mourachko, M. W. Noel, and T. F. Gallagher, Phys. Rev. A **67**, 052502 (2003).
[18] J. Han, Y. Jamil, D. V. L. Norum, P. J. Tanner, and T. F. Gallagher, Phys. Rev. A **74**, 054502 (2006).
[19] P. Pillet, R. Kachru, N. H. Tran, W. W. Smith, and T. F. Gallagher, Phys. Rev. A **36**, 1132 (1987).
[20] D. Tong, S. M. Farooqi, J. Stanojevic, S. Krishnan, Y. P. Zhang, R. Côté, E. E. Eyler, and P. L. Gould, Phys. Rev. Lett. **93**, 063001 (2004).
[21] J. H. Shirley, Phys. Rev. **138**, B979 (1965).
[22] T. G. Walker and M. Saffman, Phys. Rev. A **77**, 032723 (2008).
[23] J. Han and T. F. Gallagher, Phys. Rev. A **77**, 015404 (2008).
[24] M. W. Noel (private communication).
[25] M. Brune (private communication).
[26] R. C. Teixeira, C. Hermann-Avigliano, T. L. Nguyen, T. Cantat-Moltrecht, J. M. Raimond, S. Haroche, S. Gleyzes, and M. Brune, Phys. Rev. Lett. **115**, 013001 (2015).